PHYSICAL REVIEW C
NUCLEAR PHYSICS

THIRD SERIES, VOLUME 32, NUMBER 3 SEPTEMBER 1985

Microscopic optical model analysis of nucleon scattering from light nuclei

J. S. Petler, M. S. Islam, and R. W. Finlay
Ohio University, Athens, Ohio 45701

F. S. Dietrich
Lawrence Livermore National Laboratory, Livermore, California 94550
(Received 3 May 1985)

Differential cross sections for neutron elastic scattering from ^{12}C, ^{14}N, ^{16}O, and ^{27}Al have been measured in the energy range 18—26 MeV. These data, together with previously published neutron and proton data for these nuclei and for ^{12}C in the energy region 20 to 65 MeV, have been analyzed in terms of two microscopic optical potentials. The spherical potential derived from the work of Jeukenne, Lejeune, and Mahaux provides a consistent representation of the differential data, provided the imaginary central potential is renormalized. Predictions from the interaction of Brieva and Rook give less satisfactory agreement. In particular, there is a significant overprediction of the forward angle data below ~25 MeV and an underprediction above ~35 MeV.

I. INTRODUCTION

Elastic neutron and proton scattering from nuclei is most frequently described in terms of complex optical potential models. These are often phenomenologically based, using standard form factors for the potential wells, with the depths and geometries determined by fitting experimental data. However, the potentials can be derived from the more fundamental effective nucleon-nucleon interaction by applying folding integrals incorporating a local density approximation (LDA). In our previous investigations, microscopic optical potentials derived from both the nuclear matter calculations of Jeukenne, Lejeune, and Mahaux (JLM),[1-4] and the energy and density dependent t matrix of Brieva and Rook[5-9] have had success at describing nucleon scattering from medium (^{54}Fe and ^{56}Fe) (Ref. 10) and heavy (^{208}Pb and ^{209}Bi) nuclei.[11,12] The models have also been tested for neutron scattering over a wide mass range ($A=9$—209) at 14 MeV.[13] In the present work we attempt an extensive test of the models for several light nuclei over a wide energy range for both protons and neutrons. This extension to light nuclei constitutes a severe test of the applicability of the local density approximation that is used to obtain optical potentials for finite nuclei from calculations performed in "infinite nuclear matter." Phenomenological spherical optical model analyses of light nuclei tend to produce parameters that are different from the standard "global" values, and descriptions of the angular distributions are generally poorer. This is sometimes attributed to using a Woods-Saxon or derivative Woods-Saxon form for the potentials. The potentials calculated in the microscopic analysis do not have this built-in assumption. Light nuclei have the property of low level densities, and hence resonance structure is often present. Since both models are smoothly energy dependent, the present analysis is concentrated above ~18 MeV where the measured total cross sections show reasonably smooth behavior.

II. EXPERIMENTAL

The neutron scattering data presented in this paper were taken using the Ohio University time-of-flight facility[14] in several experiments over a period of about two years. Neutrons of the required energy were produced in a gas cell of 3 cm length using the $^3H(d,n)$ source reaction, and the samples were irradiated by the 0° flux. The scattered neutrons were detected by an array of seven NE213 liquid scintillation counters positioned in a time-of-flight tunnel. Overall normalization is achieved using an additional proton-recoil scintillator as a monitor, fixed in relation to the neutron source, and by frequent measurements in which the sevenfold array views the 0° flux of neutrons from the gas cell with the scattering sample removed.

Several different scattering samples were used, each in the form of a right-circular cylinder. Details of the samples and energies investigated are given in Table I. The oxygen data were obtained using a sample of aluminum oxide formed as a high density ceramic with the attendant advantage of an increase in number density over that which can be obtained with a water sample. Similarly, the nitrogen data were taken using an aluminum nitride sam-

TABLE I. Sample properties and incident neutron energies.

Nucleus	Sample	Dimensions height (cm)	Dimensions diam (cm)	mass (g)	Neutron energies (MeV)
^{13}C	98.02% isotopically enriched graphite powder in an aluminum can	3.23	3.58	40.75	24
^{14}N	AlN ceramic	3.28	2.51	16.66	20,25
^{16}O	Al_2O_3 ceramic	2.89	2.62	26.82	18,20,22,26
^{27}Al	Al metal	2.89	2.62	30.17	18,20,22,26
		3.28	2.51	32.13	20,25

ple. For these experiments, "background" spectra were obtained by measuring an aluminum sample of the same height and diameter, with the mass adjusted to that of the aluminum in the ceramic by drilling several small holes. Differential cross sections for aluminum were thus obtained parasitically by performing an additional measurement of the background signal arising from air-scatter and from the nylon sample support strings at each angle. The ^{13}C sample was a fine powder, enriched to 98.0%, encased in a thin aluminum can, with an empty container of the same mass acting as sample-out.

Typical time of flight spectra are shown in Fig. 1. The AlN spectrum [Fig. 1(a)] shows both the sample-in and monitor-normalized sample-out spectra. The oxide spectrum [Fig. 1(b)] has had the $^{27}Al(n,n')$ spectrum subtracted. The elastic cross sections were obtained by summing over the peak region in each spectrum and then correcting for a number of well-understood effects such as multiple scattering, neutron attenuation within the sample, finite

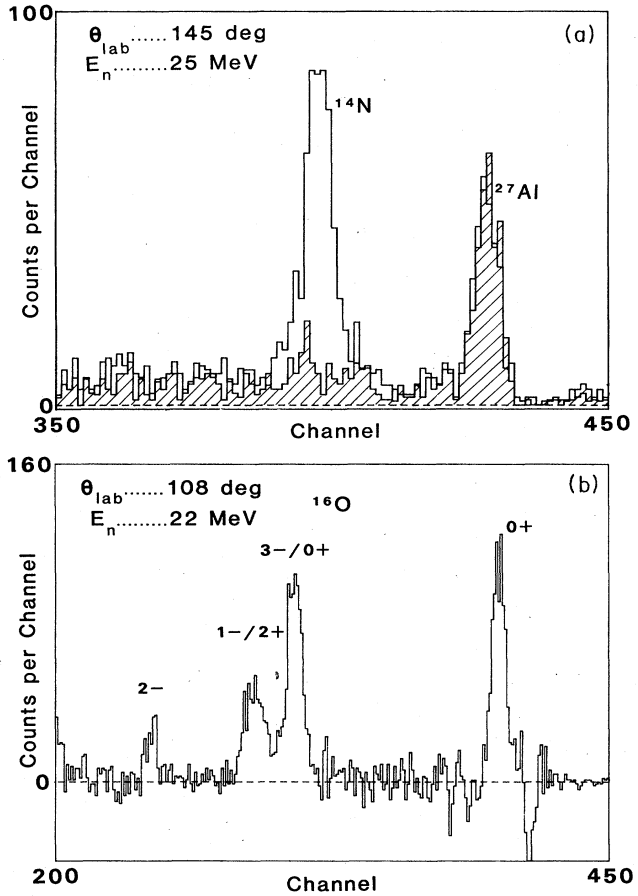

FIG. 1. (a) Typical time of flight spectra obtained for the AlN sample at 25 MeV. The hatched area is the monitor-normalized $^{27}Al(n,n')$ spectrum. (b) Time of flight spectrum for $^{16}O(n,n')$ at 22 MeV. The scattering arising from $^{27}Al(n,n')$ has been subtracted.

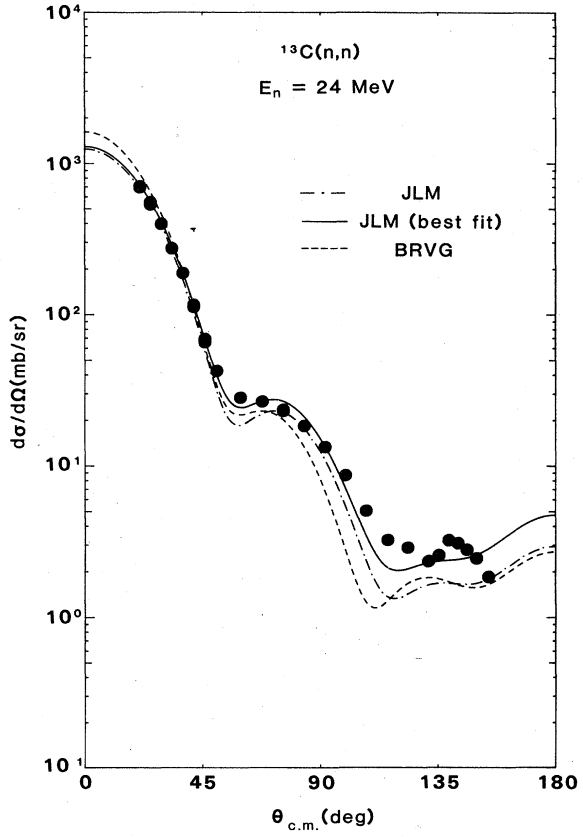

FIG. 2. Microscopic optical model calculations of $^{13}C(n,n)$ at $E_n=24$ MeV. The dashed and dot-dashed curves correspond to the BRVG and JLM models with no renormalization of the potentials. The solid curve shows the effect searching for the optimum λ_w while fixing λ_v at unity.

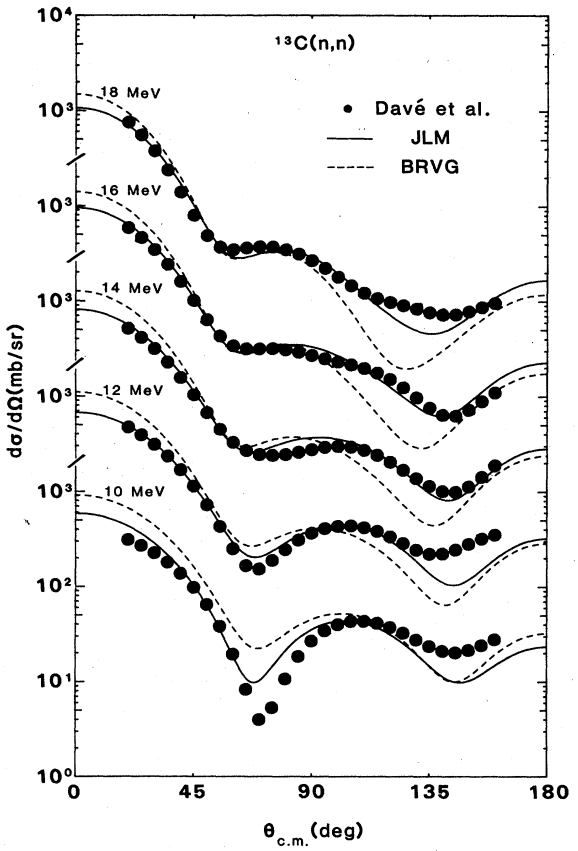

FIG. 3. JLM ($\lambda_w=0.8$) and BRVG calculations of ^{13}C(n,n). The experimental data are from Ref. 26.

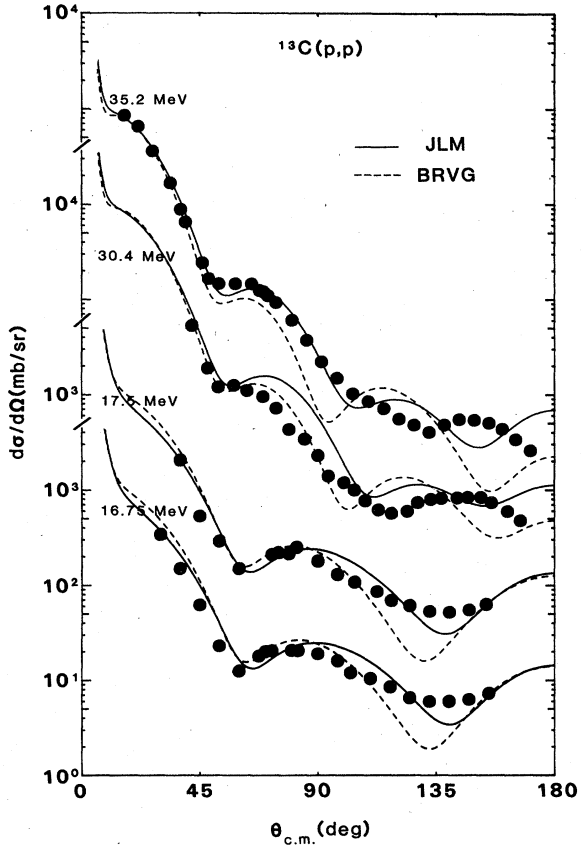

FIG. 4. JLM ($\lambda_w=0.8$) and BRVG calculations for proton scattering from ^{13}C. The data are those of Refs. 27 (16.75, 17.5 MeV), 28 (30.4 MeV), and 29 (35.2 MeV).

geometry, variation in detection efficiency with energy, and the energy and time spreads in the incident deuteron beam. The Monte Carlo code EFFIGY (Ref. 15) was used to calculate these corrections. The effect of attenuation within the samples can be seen in Fig. 1(b), where the region that contained the aluminum peak, to the right of the oxygen elastic peak, is negative. This effect can be accounted for in EFFIGY provided the aluminum cross section is known.

A correction of 1—3% for the anisotropy of the ^{3}H(d,n) reaction is also applied. This arises because the detectors at 0° subtend a smaller solid angle than the samples. This correction depends on the neutron energy and source-to-sample distance, which in this series of experiments varied between 12 and 18 cm.

Two separate experiments were performed at 20 MeV with the Al_2O_3 sample. The cross sections extracted from these data were in good agreement and were combined to produce the final data set. Nitrogen cross sections were also obtained at 20 MeV and, hence, there were three sets of ^{27}Al elastic cross sections. Where the data had been

TABLE II. Phenomenological spherical optical model parameters obtained in the present work. A Woods-Saxon form for the real potential is used, and the imaginary potential includes Woods-Saxon and derivative Woods-Saxon terms. All lengths are given in fm, potentials in MeV, and E is the laboratory neutron energy in MeV. (I) denotes that the geometrical parameters were obtained from Ref. 44 and were fixed. (II) denotes parameters obtained by searching on geometrical parameters as well as the potentials.

Nucleus	E_n	V_R	r_R	a_R	W_V	W_D	r_I	a_I
^{14}N[a]	20	47.41	1.20	0.605		5.34	1.39	0.499
	25	45.91	1.20	0.605		5.13	1.39	0.499
^{16}O[b]	<21	$53.51-0.297E$	1.15	0.646		$6.49-0.31(21-E)$	1.38	0.473
	>21	$53.51-0.297E$	1.15	0.646	$0.167(E-21)$	$6.49-0.17(E-21)$	1.38	0.473
^{27}Al[a](I)		$51.55-0.308E$	1.18	0.64	$0.175(E-15)$	$6.07-0.10(E-15)$	1.26	0.58
(II)		$49.16-0.289E$	1.22	0.606	$0.207(E-15)$	$6.67-1.12(E-15)$	1.29	0.509

[a]For ^{14}N and ^{27}Al the spin orbit potentials were taken to be $V_{so}=6.0$ MeV, $r_{so}=1.01$, $a_{so}=0.50$.
[b]For ^{16}O the spin orbit potentials were taken from Ref. 37: $V_{so}=4.31$ MeV, $r_{so}=1.11$, $a_{so}=0.45$.

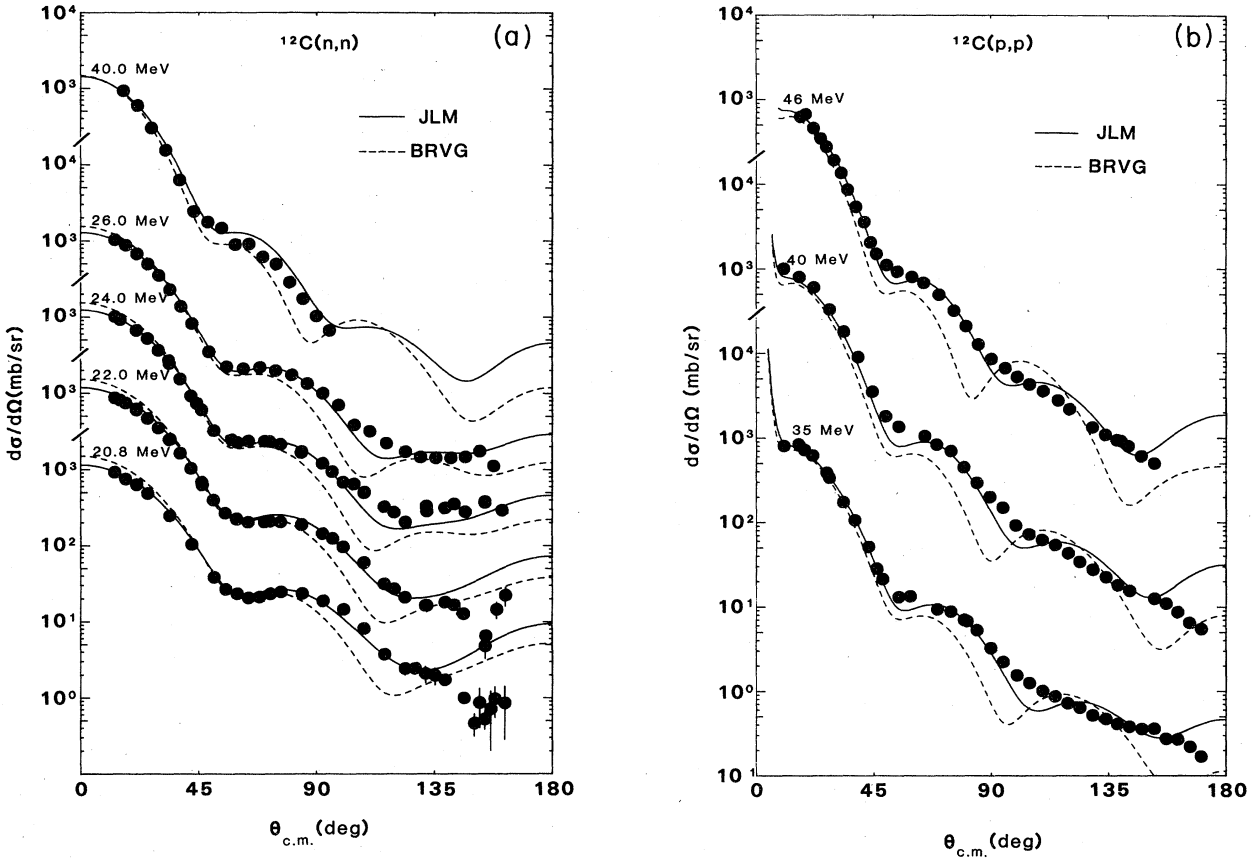

FIG. 5. (a) Microscopic optical model calculations of ^{12}C(n,n). The data are from Refs. 30 (20—26 MeV) and 31 (40 MeV). (b) JLM and BRVG calculations of ^{12}C(p,p) compared with the data of Refs. 32 (35, 40 MeV) and 33 (46 MeV). (c) JLM and BRVG calculations of ^{12}C(p,p) compared with the data of Ref. 32 (30 MeV) and Ref. 34 (65 MeV).

obtained at the same angle, the resulting cross sections were averaged.

III. ANALYSIS

A. Calculational procedure

Two spherical microscopic optical potentials are investigated in the present work, that of Jeukenne *et al.*,[1–4] based on Reid's hard core interaction,[16] and the Yukawa parametrization by von Geramb[9] of the effective interaction of Brieva and Rook[5–8] (BRVG), which is derived from the Hamada-Johnston potential.[17] In both sets of calculations the spin orbit potential is taken from the work of Bertsch *et al.*[18] and is real and density and energy independent. The details of the present calculations are identical to those described by Mellema *et al.*[10] and by Dietrich *et al.*[11] with the additional refinement that the exchange contributions in the BRVG calculations are computed with a complex self-consistent wave number calculated from the local kinetic energy and the complex optical potential. The overall effect of this adjustment, also used by Hansen *et al.*,[13] is to introduce a very small imaginary spin orbit potential and to reduce the imaginary potential volume integral by ~20%.

The calculational procedures require the nuclear ground state matter densities as input. The proton point-nucleon density ρ_p is obtained by deconvoluting the proton charge distribution from the charge density measured by electron

TABLE III. Results of χ^2 searched on ^{16}O(n,n) data forward of 90° for the effective interactions derived from the Hamada-Johnston potential.

	Brieva and Rook				Yamaguchi *et al.*			
E_n (MeV)	λ_v	λ_w	χ^2 initial	χ^2 final	λ_v	λ_w	χ^2 initial	χ^2 final
18.0	1.11	1.21	77.49	39.6	0.99	0.54	96.2	2.7
20.0	1.19	1.46	201.9	79.4	1.02	0.66	68.3	9.6
22.0	1.14	1.16	26.9	15.4	1.01	0.60	57.7	2.4
24.0	1.06	0.81	97.1	31.7	1.00	0.57	232.4	1.7
26.0	1.03	1.05	14.9	14.5	0.97	0.60	49.7	1.0

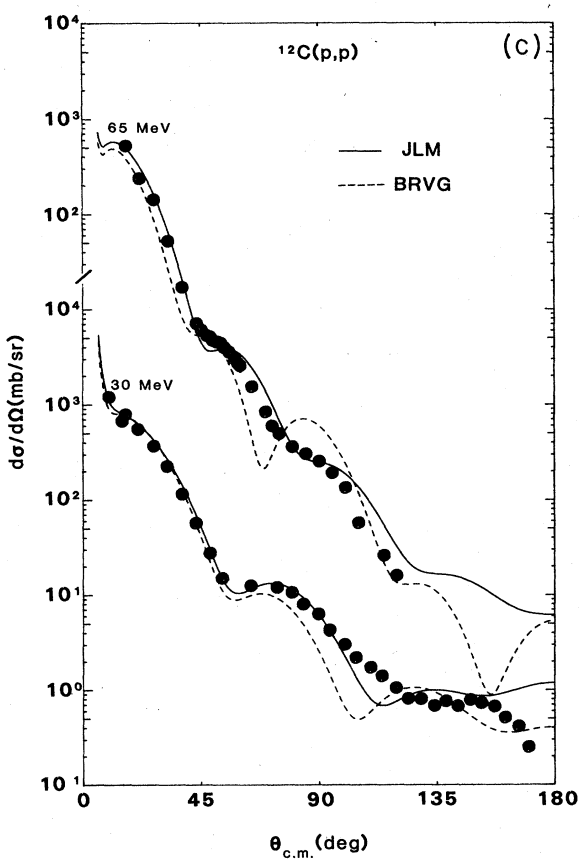

FIG. 5. (*Continued*).

scattering. The neutron density ρ_n is assumed to be the same as for protons for the self-conjugate nuclei and, for the others, was determined by applying the assumption $\rho_n=(N/Z)\rho_p$.

The results of several different (e,e) analyses have been used. The model independent analysis (MIA) of Sick[19] was the primary input to all of the ^{12}C data presented in this paper. The MIA has the advantage that no *a priori* assumptions have been put on the form of the charge density and hence the form of the matter distribution. However, it was found that somewhat different expressions for the charge density, for example, the modified harmonic oscillator description of Sick and McCarthy[20] and the Fourier-Bessel expansion of Reuter *et al.*,[21] gave essentially the same predicted differential cross sections. Calculations for the other nuclei investigated in the present work use the (e,e) data of Ref. 22 for ^{13}C, of Ref. 23 for ^{14}N, of Ref. 20 for ^{16}O, and of Ref. 24 for ^{27}Al.

The real and imaginary central potentials and the spin-orbit potential are calculated from the nucleon density distributions and the effective interaction by a folding procedure. A "midpoint LDA" was used in which the density at which the effective interaction takes place is evaluated by the arithmetic mean of the projectile and target positions. The consequences of choosing different prescriptions for the LDA are discussed in Ref. 10. The nuclear matter optical potentials of JLM are treated as an effective interaction by dividing by the density[3] and by smearing by a Gaussian form factor with an effective range parameter (t in Ref. 3) of 1.0 fm for both the real and imaginary potentials. This value was empirically found in the work of Mellema *et al.*,[10] which also used a "midpoint LDA," and was kept fixed in the present work.

The potentials calculated by the folding integrals are then used in a spherical optical-model program to calculate elastic scattering angular distributions as well as total and reaction cross sections. In our previous analyses[10,11,25] using microscopic folding models, normalization parameters were introduced to adjust the calculated optical potentials:

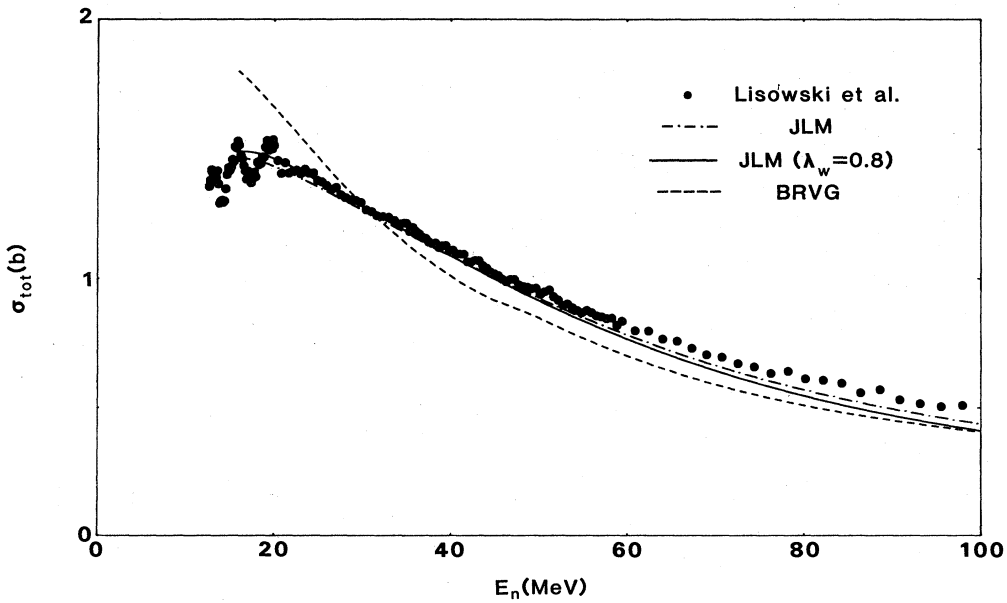

FIG. 6. Neutron total cross sections predicted by the BRVG and JLM models for ^{12}C + n compared with the experimental values of Lisowski *et al.* (Ref. 35).

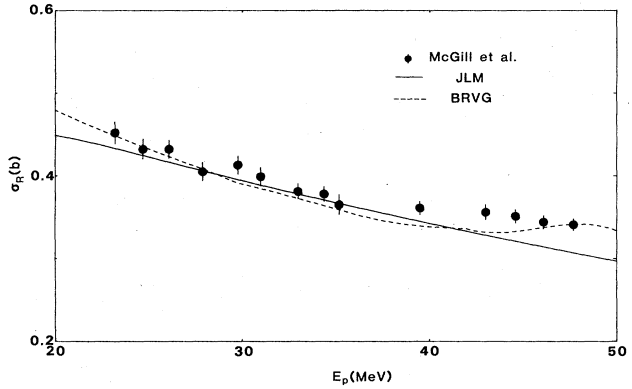

FIG. 7. The $^{12}C + p$ reaction cross section data of McGill *et al.* (Ref. 36) and the corresponding JLM and BRVG calculations.

$$U = \lambda_v V + i\lambda_w W + \lambda_{so} V_{so} \ .$$

The normalization for the real central potential was found to be within 10% of unity for both lead[11] and the iron isotopes.[10] In both analyses, significant (up to ~40%) energy-dependent normalizations were required for the imaginary potential. Whenever the normalization coefficients $\lambda_{v,w}$ were searched (by a least squares procedure) in the present work, only the differential cross section data for $\theta < 100°$ were included in the search. This precaution was taken to avoid undue weighting of the results by the back-angle data, which for light nuclei are frequently very difficult to describe with any potential-scattering picture.

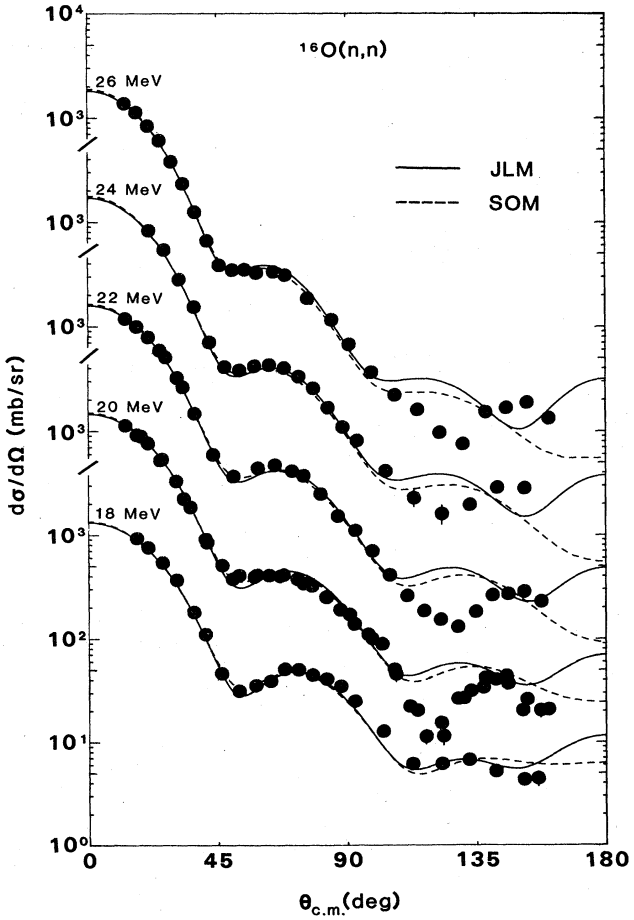

FIG. 8. Comparison of JLM and phenomenological optical model calculations for ^{16}O(n,n). The data at 24 MeV are those of Ref. 38.

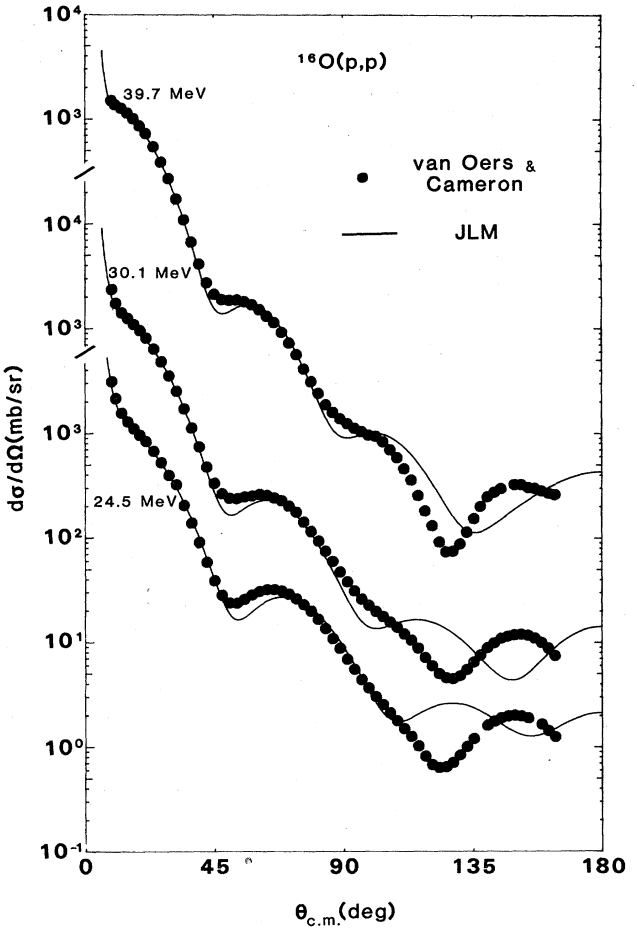

FIG. 9. JLM calculations of ^{16}O(p,p). The data are from Ref. 42.

It was found that for the BRVG calculations only small improvements in agreement with the angular distributions could be achieved by allowing the λ_v and λ_w to vary. The resulting values of λ_v and λ_w were widely scattered and displayed no systematic variation with energy. Hence, in most of the figures shown in this paper only the unadjusted BRVG calculations are presented. In contrast, when using the JLM central potential, adjustment produced dramatic improvements. Searches performed on ^{12}C and ^{13}C differential data between 20 and 65 MeV consistently yielded λ_v within 10% of unity and λ_w between 0.72 and 0.95. There was no consistent evidence for the need to normalize the real potential, so λ_v was fixed at 1.0 and searches were performed for the optimum values of λ_w only. The overall quality of fit (determined by χ^2) was similar to that of the two-parameter search with resulting values of λ_w being between 0.7 and 0.9. A compromise

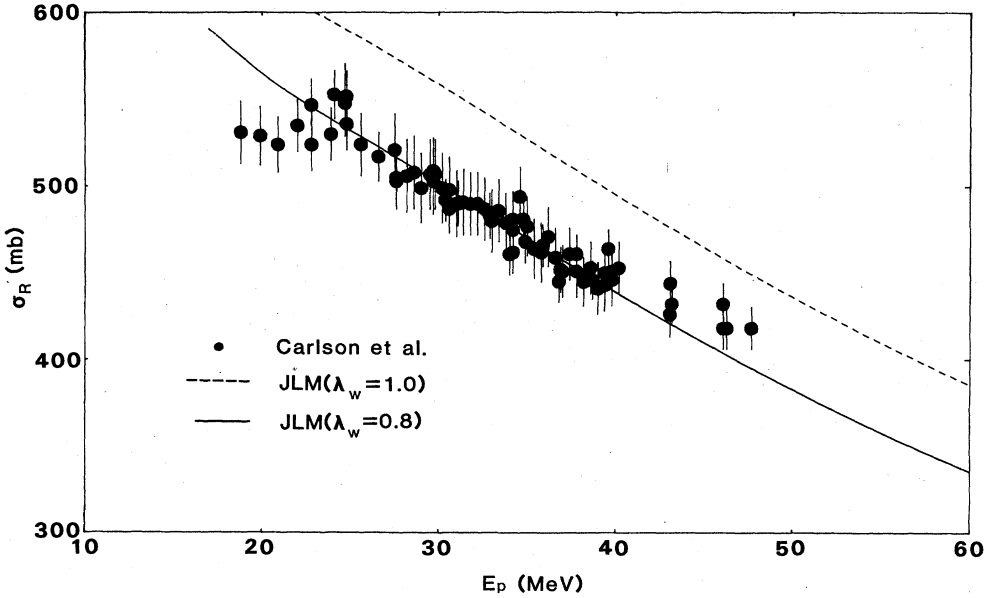

FIG. 10. Comparison between JLM ($\lambda_w=1.0$) and JLM ($\lambda_w=0.8$) calculations of the $^{16}O + p$ reaction cross section and the experimental results of Ref. 43.

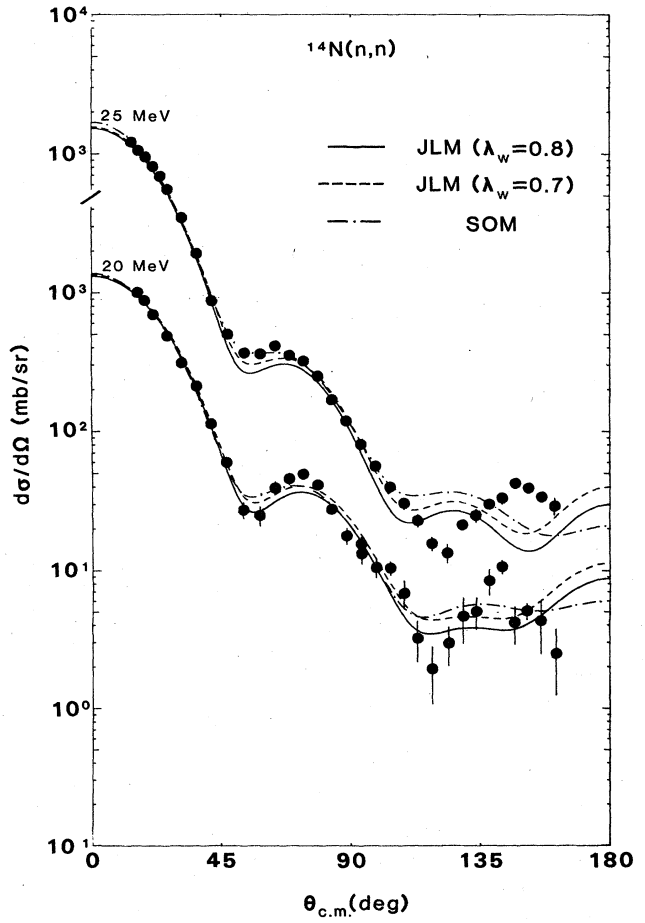

FIG. 11. JLM ($\lambda_w=0.8$) (solid), JLM ($\lambda_w=0.7$) (dashed), and phenomenological optical model descriptions of ^{14}N(n,n).

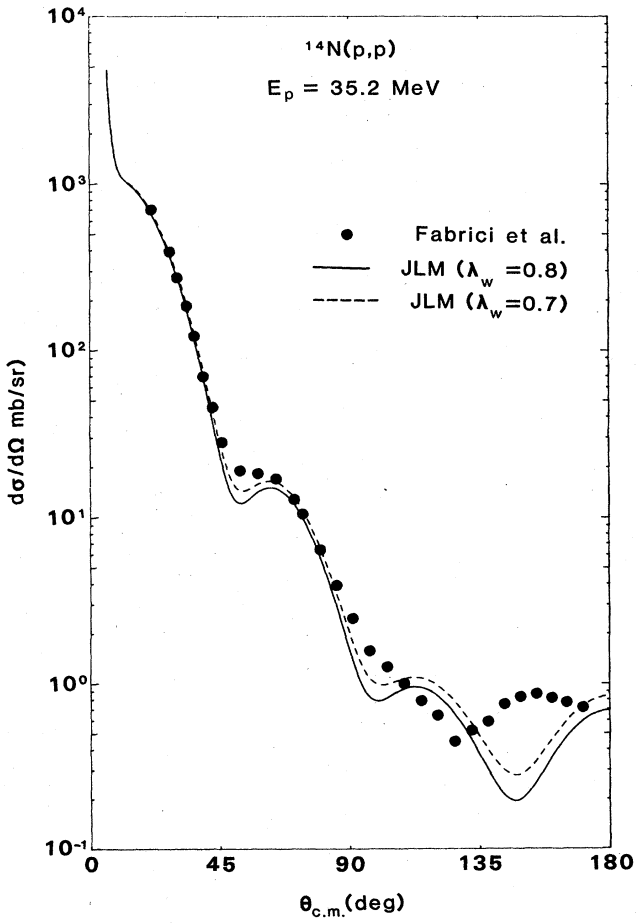

FIG. 12. JLM calculations of ^{14}N(p,p) at 35.2 MeV compared with the data of Ref. 29. The dashed line is for $\lambda_w=0.7$ and the solid curve is for $\lambda_w=0.8$.

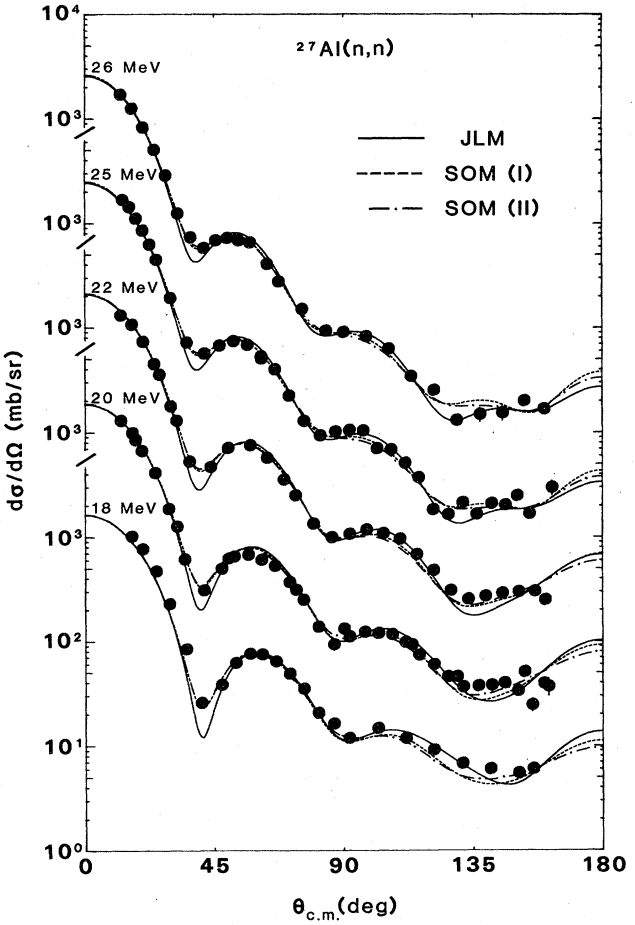

FIG. 13. Microscopic and phenomenological optical model calculations of ^{27}Al(n,n). The imaginary normalization for the JLM calculations (solid curve) was set at 0.925. The dash-dot and dotted curves correspond to sets I and II in Table II, respectively.

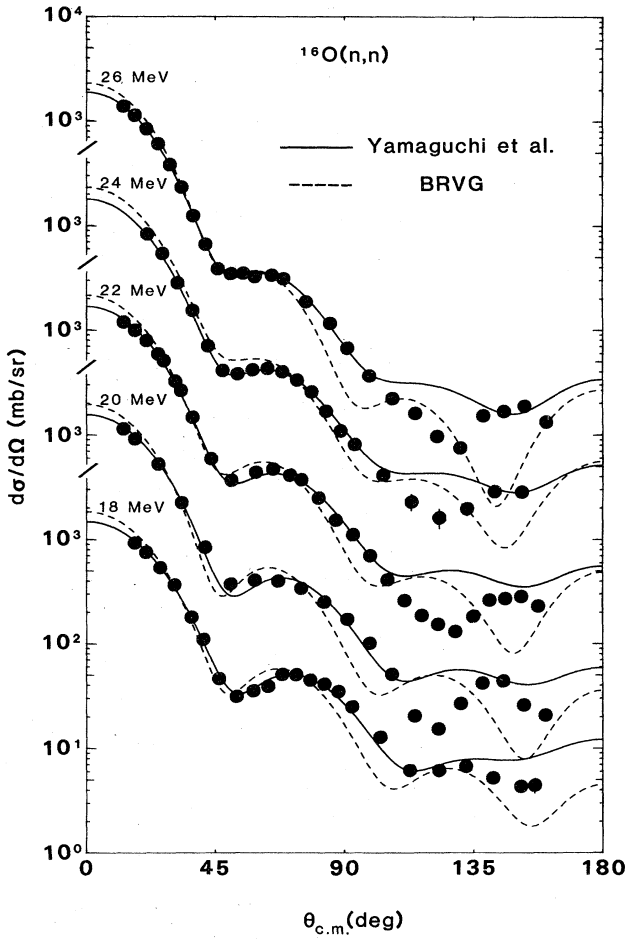

FIG. 14. A comparison of microscopic calculations based on the Hamada-Johnston potential. The dashed and solid lines are based on the effective interactions of Brieva and Rook and of Yamaguchi *et al.*, respectively. The 24 MeV data are from Ref. 38.

value of 0.8 was chosen, and except where noted all the curves with the JLM interaction were calculated with $\lambda_v = 1.0$ and $\lambda_w = 0.8$.

B. ^{13}C

Figure 2 shows unadjusted predictions of ^{13}C(n,n) at 24 MeV for both JLM and BRVG. The BRVG calculations overpredict the measured cross section at angles $< 30°$, lie under the data at larger angles, and the diffraction minima tend to be deeper than experimentally observed. It was found for these data that only slight improvements could be achieved by allowing λ_v and λ_w to vary. For example, for the data shown in Fig. 2, χ^2 went from 61.8 to 50.1, χ^2 being determined only for data at $\theta < 100°$, and the deficiencies mentioned above were still present. The corresponding values of λ_v and λ_w were 1.11 and 0.98, respectively. The overprediction of the cross section at forward angles by the BRVG calculations, and hence the overestimate of the total cross section, was also noted for iron by Mellema *et al.*[10] and by Hansen *et al.*,[13] who showed that the overprediction gets worse as the target mass number decreases.

In contrast to the BRVG calculations, the prediction of the JLM model (dashed-dot line) shows good agreement with the data at forward angles, although it also lies below the data beyond $\sim 45°$. A search on λ_v and λ_w performed with this model produced optimum values of $\lambda_v = 1.01$ and $\lambda_w = 0.82$. The solid curve in Fig. 2 is the result of fixing λ_v at 1.0 and only searching on λ_w. The value of λ_w was 0.80, and the χ^2 for this fit is a factor of 3 better than the unadjusted prediction and comparable to a seven-free-parameter phenomenological spherical optical model fit (not shown).

Figure 3 shows the results of JLM and BRVG calculations of ^{13}C(n,n) between 10 and 18 MeV together with the data of Dave *et al.*[26] The JLM calculations incorporate a 20% reduction in the imaginary central potential, while the BRVG calculations correspond to the unadjusted prediction. As was noted above, no significant improvements in fit could be obtained by allowing λ_v and λ_w to vary in the BRVG calculations. The overprediction at forward angles by the BRVG model becomes more severe at lower neutron energies. The results of the JLM calcu-

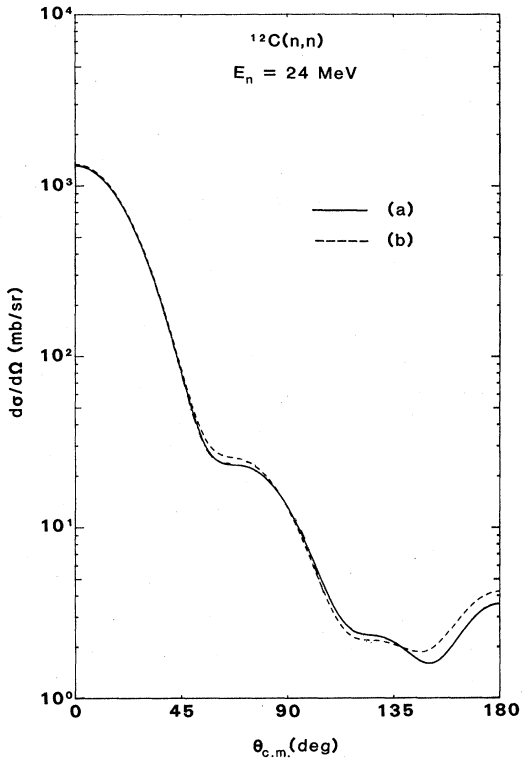

FIG. 15. Optical model calculations of ^{12}C(n,n) at 24 MeV. See the text for details of the calculations.

lations at the four highest energies give agreement that can be favorably compared to the energy-dependent spherical optical model derived in Ref. 26.

The isospin consistency of these microscopic calculations was discussed in Refs. 10 and 11 and is illustrated in Fig. 4, where ^{13}C(p,p) data from Weller *et al.*,[27] Greaves *et al.*,[28] and Fabrici *et al.*[29] are compared with JLM ($\lambda_w = 0.8$) and BRVG calculations. The BRVG results show the same trends noted in the neutron scattering data, an overprediction at forward angles that decreases with increasing energy and an angular distribution that is too diffracted. Apart from the results at 30.4 MeV, there is reasonable agreement between the JLM predictions and the scattering data. We note that the stated normalization uncertainty in Ref. 28 was $\pm 20\%$ and that difficulties with the isotopic and chemical purity of the target were mentioned. Visual inspection of Fig. 4 suggests that an upward renormalization of the 30.4 MeV data by about this amount would result in better overall agreement with the calculation.

C. ^{12}C

Although no new ^{12}C data are presented in this paper, there is a large amount of published (n,n), (p,p), total and reaction cross section data for this nucleus. It is instructive to see if the results of the microscopic calculations show the same behavior as observed in ^{13}C. Figure 5 shows the results of BRVG (unadjusted) and JLM ($\lambda_w = 0.8$) for neutron and proton scattering at a number of energies between 20 and 65 MeV. The JLM results are consistently good and those using BRVG show the same problems as encountered in the ^{13}C analysis. The change in the forward angle cross sections in the BRVG calculations, from overprediction to underprediction as the energy increases, can be seen in Fig. 5 and in the calculated total cross section (Fig. 6). The total cross section calculated with the JLM interaction ($\lambda_w = 0.8$) also lies below the data of Lisowski *et al.*[35] above ~ 35 MeV, whereas the agreement with experiment between 15 and 30 MeV is satisfactory. The unadjusted JLM calculations (dot-dashed) also lie below the data at all energies. To achieve agreement with the measured total cross sections, it would be sufficient to normalize the real potential upward by 5% at 50 MeV and by 12% at 80 MeV.

Comparison with the reaction cross section is particularly useful, as this quantity is very sensitive to the strength of the imaginary potential. Figure 7 shows the p + ^{12}C reaction cross section data of McGill *et al.*[36] together with the BRVG and JLM ($\lambda_w = 0.8$) calculations. The normalized JLM and the BRVG calculations both describe these data quite well. The cross sections predicted by the unadjusted JLM calculations lie above the experimental data by 50 mb.

D. ^{16}O

The ^{16}O(n,n) cross sections measured in the present work are shown in Fig. 8, except for the data at 24 MeV, which are those of Grabmayr *et al.*[38] The solid lines in Fig. 8 are JLM calculations ($\lambda_w = 0.8$) and the dashed lines are from the phenomenological spherical optical potential given in Table II. The phenomenological parameters were found by simultaneously fitting the cross sections at $\theta < 100°$ for the five data sets, requiring a common geometry and linear energy dependences of the real and imaginary potential wells. The more extensive data set produced by this work has required a slight modification of the geometrical parameters presented by Grabmayr *et al.*[38] In particular, r_R and a_I need to be 1.15 and 0.473, respectively, compared to the previous values of 1.10 and 0.588. Both the microscopic and phenomenological optical model calculations provide a good description of the data forward of 100°. At all but the lowest energy, 18 MeV, the data show a deep back angle minimum that cannot be reproduced by any conventional parametrization of the spherical optical model potential or any adjustment of λ_v or λ_w in the JLM calculations. This minimum has been observed in proton scattering from several nuclei (for example, Refs. 29, 39, 40, and 41), principally in $A = 4N$ nuclei such as ^{16}O and ^{40}Ca, and has been explained in several ways: inadequacies in the Woods-Saxon parametrization, resonances in the compound nucleus,[39] coupled channel effects involving giant resonances[40] and l-dependent optical potentials.[41]

Figure 9 shows a sample of the JLM calculations for ^{16}O(p,p) together with some of the data of van Oers and Cameron.[42] The agreement between calculations and experiment is not as good as was obtained with neutrons, as the model produces a first diffraction minimum that is too deep. The comparison between the predicted reaction cross section and the experimental data from Carlson

et al.[43] (Fig. 10) shows that, at least between 22 and 45 MeV, a value of λ_w of 0.8 provides excellent agreement.

E. ^{14}N

The data measured in the present work include elastic neutron scattering from ^{14}N at two energies, 20 and 25 MeV. Figure 11 shows the results of two separate JLM calculations. The solid line is that with $\lambda_v = 1.0$ and $\lambda_w = 0.8$, the parameters that were appropriate for both the carbon isotopes and oxygen over a wide energy range. The model provides a reasonable description up to $\sim 45°$ but lies below the experimental data at the second maximum. The dashed line, which lies closer to the data, in particular at 25 MeV, is $\lambda_v = 1.0$ and $\lambda_w = 0.7$. These searched parameters, obtained by a χ^2 search on the data forward of 90°, indicate the need for a slightly larger decrease in the imaginary potential than was observed in the other nuclei. As with ^{16}O, the greatest disagreement between calculation and experiment is at angles $\sim 120°$ where a minimum is visible in the measured cross section that is not predicted in either the microscopic calculation or a phenomenological spherical optical model (dash-dot line). The phenomenological parametrization (given in Table II) was obtained by fitting both sets of neutron data simultaneously, requiring the same geometrical parameters and a difference in the real potential depth of 1.5 MeV, which corresponds to the typical $-0.3E$ energy dependence of $V(r,E)$ found in global potentials.

Similar behavior was found for proton scattering. Figure 12 shows the ^{14}N(p,p) data of Fabrici *et al.*[29] at 35.2 MeV and two JLM calculations. The dashed line corresponds to $\lambda_v = 1.0$ and λ_w of 0.70, while the solid line was obtained with a λ_w of 0.8.

F. ^{27}Al

Figure 13 shows both JLM and spherical optical model (SOM) calculations for the five neutron energies investigated. Optimum values of λ_w were between 0.87 and 0.96, with no obvious systematic variation, so in Fig. 13 a compromise value of 0.925 was used. The agreement between calculation and experiment is somewhat better than that observed earlier with the lighter nuclei. Two energy-dependent spherical optical model fits to the data are also shown in Fig. 13 and the parameters are given in Table II. The geometrical parameters were taken from the work of Whisnant *et al.*[44] and only the depths of the potential wells were searched to get set I. An optical model search code[45] as used to optimize the parameters at all the five neutron energies simultaneously, with the requirement that the potential also fit the total cross section[46] up to 80 MeV. In the work presented in Ref. 44 only a derivative Woods-Saxon imaginary potential was introduced, while in the present work a volume term was also used, with the same geometrical parameters. Further searches, allowing the geometry to vary, produced small improvements in χ^2 (set II) and the dotted curves in Fig. 13.

IV. DISCUSSION AND CONCLUSIONS

The JLM central potential has been particularly successful in describing elastic neutron and proton scattering from all the nuclei examined in this work, provided the imaginary potential is adjusted downward by a small amount by a normalization factor, λ_w. The deficiencies observed in phenomenological analyses using a standard spherical optical potential, i.e., the inability to fit the back-angle minima in oxygen and nitrogen, are still present. For oxygen and the carbon isotopes λ_w was found to be essentially constant at 0.8 for all the angular distribution data examined. Reaction cross section data also demand this value. In the ^{12}C total cross section there is a suggestion that above about 35 MeV renormalization of the real central potential may be required. The λ_w values appropriate for ^{14}N and ^{27}Al are 0.7 and 0.925, respectively.

The calculations based on the BRVG interaction are less successful than those with the JLM in reproducing the shapes of the angular distributions and the energy dependence of the total cross sections. Moreover, the fitted normalizing parameters for the BRVG interaction show significant scatter, which is a further indication that the calculated angular distributions are not well matched to the data. As was discussed in Ref. 10, these difficulties are probably associated with an anomalous shape predicted by the BRVG interaction for the real potential in the region of the nuclear surface. Recently, Yamaguchi *et al.*[47] have made available another interaction which, like the BRVG, is based on the Hamada-Johnston potential. Comparison of the scattering predicted by this interaction with that from BRVG is important in determining whether the problems encountered in using the BRVG interaction originate with the two-nucleon potential, or are associated with the techniques used to generate an effective interaction. A detailed comparison of results calculated for proton scattering from ^{12}C and ^{14}C using the two interactions is presented in a related work;[48] here, we show results for neutron scattering from ^{16}O. The angular distributions are presented in Fig. 14 and the normalizing parameters in Table III. As discussed in Ref. 48, the spin-orbit interaction of Yamaguchi *et al.* has been normalized upward by 30%. The λ_w values obtained with the effective interaction of Yamaguchi *et al.* are consistent with unity, whereas a large reduction in the imaginary potential (about 40%) is required. The resulting parameters show no obvious energy dependences. The BRVG calculations, as well as yielding less satisfactory agreement with the data, produce values for the normalizing parameters that are widely scattered. Since the same nuclear matter densities and method for applying the LDA have been used for the two sets of calculations, the much improved agreement between experiment and calculation obtained with the Yamaguchi *et al.* effective interaction seems to indicate that the difficulties with BRVG do not stem from the Hamada-Johnston potential.

We address one further uncertainty, that of coupled-channel effects in deformed nuclei. ^{12}C is well known to have a large permanent deformation in the ground state,[32]

and strongly coupled excited levels at 4.43 MeV (2^+ of the ground-state rotational band) and at 9.65 MeV (3^- octupole vibration). In Fig. 15 we show results of phenomenological calculations performed to estimate the effect that channel coupling and deformation of the central potential might have on the elastic distributions predicted by the microscopic folding model calculations. Meigooni *et al.*[49] have recently completed an extensive analysis of collective modes in ^{12}C excited by neutron scattering, and the form of the deformed optical potential used in these calculations was taken from that work. The solid line is a rotational-band calculation[50] with $\beta_2=-0.61$ and $\beta_4=0.05$, in which the ground, 2^+ (4.43 MeV), and 4^+ (14.08 MeV) states were included. All couplings allowed by the rotational model were calculated. The dashed line results from deforming the potential exactly as for the previous case, but setting all of the couplings between states to zero. The absorptive potential was increased by 30% to bring the forward-angle cross sections into agreement with the full calculation. Since the target spin is zero, this calculation is thus a spherical optical-model calculation, in which the projectile senses only the monopole (spherically symmetric) component of the deformed potential. The restricted calculation is analogous to the present folding-model calculations, since the densities employed are based on empirical results from electron scattering, which senses only the monopole part of the deformed charge distribution. The small differences between the solid and dashed curves are, therefore, a measure of the error incurred by the neglect of channel coupling. We conclude that for elastic scattering from spin-zero nuclei, the most important effects of deformation are included in the empirically-determined densities.

In summary, the success achieved in the microscopic analyses indicates the utility, even in nuclei as light as carbon, of the local density approximation and the folding model. Agreement with the shapes of angular distributions is nearly as good as for phenomenological fits in which the geometrical parameters are varied arbitrarily. It is particularly gratifying to note that the energy and mass dependence of the imaginary-potential strength is predicted rather accurately by the JLM potentials over the entire range of data considered in this work.

ACKNOWLEDGMENTS

We would like to thank John O'Donnell for adapting the codes used in these analyses to the Ohio University computer system. One of us (J.S.P.) would like to thank Dr. S. Mellema for many helpful discussions. The experimental data could not have been obtained without the aid of J. D. Sturbois, D. E. Carter, and the rest of the accelerator laboratory personnel. This investigation was supported by PHS Grant No. CA-25193 awarded by the National Cancer Institute, DHHS. Additional support was obtained from Lawrence Livermore National Laboratory under Contract No. W-7405-ENG-48 with the U.S. Department of Energy and from the National Science Foundation under Grant No. PHY-8108456.

[1]J.-P. Jeukenne, A. Lejeune, and C. Mahaux, Phys. Rev. C **10**, 1391 (1974).
[2]J.-P. Jeukenne, A. Lejeune, and C. Mahaux, Phys. Rev. C **15**, 10 (1977).
[3]J.-P. Jeukenne, A. Lejeune, and C. Mahaux, Phys. Rev. C **16**, 80 (1977).
[4]A. Lejeune, Phys. Rev. C **21**, 1107 (1980).
[5]F. A. Brieva and J. R. Rook, Nucl. Phys. **A291**, 299 (1977).
[6]F. A. Brieva and J. R. Rook, Nucl. Phys. **A291**, 317 (1977).
[7]F. A. Brieva and J. R. Rook, Nucl. Phys. **A297**, 206 (1978).
[8]F. A. Brieva and J. R. Rook, Nucl. Phys. **A307**, 493 (1978).
[9]*Lecture Notes in Physics 89, Microscopic Optical Potentials,* edited by H. V. von Geramb (Springer, New York, 1979).
[10]S. Mellema, R. W. Finlay, F. S. Dietrich, and F. Petrovich, Phys. Rev. C **28**, 2267 (1983).
[11]F. S. Dietrich, R. W. Finlay, S. Mellema, G. Randers-Pehrson, and F. Petrovich, Phys. Rev. Lett. **51**, 1629 (1983).
[12]J. R. M. Annand, R. W. Finlay, and F. S. Dietrich, submitted to Nucl. Phys.
[13]L. F. Hansen, F. S. Dietrich, B. A. Pohl, C. H. Poppe, and C. Wong, Phys. Rev. C **31**, 111 (1985).
[14]R. W. Finlay, C. E. Brient, D. E. Carter, A. Marcinkowski, S. Mellema, G. Randers-Pehrson, and J. Rapaport, Nucl. Instrum. Methods **198**, 197 (1982).
[15]The code EFFIGY, H. H. Hogue, Ph.D. dissertation, Duke University, 1977 (unpublished).
[16]R. V. Reid, Ann. Phys. (N.Y.) **50**, 411 (1968).
[17]T. Hamada and I. D. Johnston, Nucl. Phys. **34**, 382 (1962).
[18]G. Bertsch. J. Borysowicz, H. McManus, and W. G. Love, Nucl. Phys. **A284**, 399 (1977).
[19]I. Sick, Nucl. Phys. **A218**, 509 (1974).
[20]I. Sick and J. S. McCarthy, Nucl. Phys. **A150**, 631 (1970).
[21]W. Reuter, G. Fricke, K. Merle, and H. Miska, Phys. Rev. C **26**, 806 (1982).
[22]J. Heisenberg, J. S. McCarthy, and I. Sick, Nucl. Phys. **A157**, 435 (1970).
[23]E. B. Dally, M G. Croissiaux, and B. Scheitz, Phys. Rev. C **2**, 2057 (1970).
[24]R. M. Lombard and G. R. Bishop, Nucl. Phys. **A101**, 601 (1967).
[25]A. Lejeune and P. E. Hodgson, Nucl. Phys. **A295**, 301 (1978).
[26]J. H. Dave, C. R. Gould, L. W. Seagondollar, C. R. Howell, R. S. Pedroni, F. O. Purser, and R. L. Walter, Nucl. Sci. Eng. **80**, 388 (1982).
[27]H. R. Weller, J. Szucs, P. G. Ikossi, J. A. Kuehner, D. T. Petty, and R. G. Seyler, Phys. Rev. C **18**, 1120 (1978).
[28]P. D. Greaves, V. Hnizdo, J. Lowe, and O. Karban, Nucl. Phys. **A179**, 1 (1972)
[29]E. Fabrici, S. Micheletti, M. Pignanelli, F. G. Resmini, R. De Leo, G. D'Erasmo, A. Pantaleo, J. L. Escudie, and A. Tarrats, Phys. Rev. C **21**, 830 (1980).
[30]A. S. Meigooni, J. S. Petler, and R. W. Finlay, Phys. Med. Biol. **29**, 643 (1984).
[31]R. P. DeVito, Ph.D. dissertation, Michigan State University, 1979 (unpublished).
[32]R. De Leo, G. D'Erasmo, A. Panteleo, M. N. Harakeh, E. Cereda, S. Micheletti, and M. Pignanelli, Phys. Rev. C. **28**, 1443 (1983).
[33]G. R. Satchler, Nucl. Phys. **A100**, 497 (1967).
[34]S. Kato, K. Okada, M. Kondo, A. Shimizu, K. Hosono, T.

Saito, M. Matsuoka, and S. Nagamachi, Nucl. Instrum. Methods **169**, 589 (1980).

[35]P. W. Lisowski, M. S. Moore, G. L. Morgan, and R. E. Shamu, in Proceedings of the International Conference on Neutron Cross Sections for Technology, edited by J. L. Fowler, C. H. Johnson, and C. D. Bowman, NBS Special Publication SP-594, 1980, p. 524.

[36]W. F. McGill, R. F. Carlson, T. H. Short, J. M. Cameron, J. R. Richardson, I. Slaus, W. T. H. van Oers, J. W. Verba, D. J. Margaziotis, and P. Dohery, Phys. Rev. C **10**, 2237 (1974).

[37]R. de Swiniarski, F. G. Resmini, D. L. Hendrie, and A. D. Bacher, Nucl. Phys. **A261**, 111 (1976).

[38]P. Grabmayr, J. Rapaport, and R. W. Finlay, Nucl. Phys. **A350**, 167 (1980).

[39]O. Karban, P. D. Greaves, V. Hnizdo, J. Lowe, N. Berovic, H. Wojciechowski, and G. W. Greenlees, Nucl. Phys. **A132**, 548 (1969).

[40]M. Pignanelli, H. V. von Geramb, and R. De Leo, Phys. Rev. C **24**, 369 (1981).

[41]R. S. Mackintosh and L. A. Cordero-L., Phys. Lett. **68B**, 213 (1977); A. M. Kobos and R. S. Mackintosh, J. Phys. G **5**, 97 (1979); **5**, 359 (1979).

[42]W. T. H. van Oers and J. M. Cameron, Phys. Rev. **184**, 1061 (1969).

[43]R. F. Carlson, A. J. Cox, J. R. Nimmo, N. E. Davison, S. A. Elbakr, J. L. Horton, A. Houdayer, A. M. Sourkes, W. T. H. van Oers, and D. J. Margaziotis, Phys. Rev. C **12**, 1167 (1975).

[44]C. S. Whisnant, J. H. Dave, and C. R. Gould, Phys. Rev. C **30**, 1438 (1984).

[45]The code OPSTAT, J. R. M. Annand, Ohio University, 1983.

[46]I. F. Bubb, S. N. Bunker, M. Jain, J. W. Leonard, A. McIlwain, K. I. Roulston, K. G. Standing, D. O. Wells, and B. G. Whitemore, Can. J. Phys. **52**, 648 (1974); M. Auman, F. P. Brady, J. A. Jungerman, W. J. Knox, M. R. McGie, and T. C. Montgomery, Phys. Rev. C **5**, 1 (1972); J. M. Peterson, A. Bratenahl, and J. P. Stoering, Phys. Rev. **120**, 521 (1960).

[47]N. Yamaguchi, S. Nagata, and T. Matsuda, Prog. Theor. Phys. (Jpn.) **70**, 459 (1983).

[48]N. L. Back, F. S. Dietrich, J. Woodworth, I. Proctor, C. Poppe, H. E. Conzett, and C. Rioux (unpublished).

[49]A. S. Meigooni, R. W. Finlay, J. S. Petler, and J. P. Delaroche submitted to Nucl. Phys.

[50]The code used was ECIS79 (J. Raynal, Saclay, unpublished).